

LIBRARY  
ROYAL AIRCRAFT ESTABLISHMENT  
BEDFORD.



MINISTRY OF AVIATION

AERONAUTICAL RESEARCH COUNCIL

CURRENT PAPERS

# Free-Flight Measurements of the Drag and Longitudinal Stability of a Transonic M-Wing Aircraft

*by*

*J. B. W. Edwards*

LONDON: HER MAJESTY'S STATIONERY OFFICE

1964

PRICE 6s 6d NET



U.D.C. No. 533.693.9 : 533.6.055 : 533.6.013.12 : 533.6.013.412 : 533.6.011.35

C.P. No. 773  
November 1963

FREE-FLIGHT MEASUREMENTS OF THE DRAG AND LONGITUDINAL STABILITY  
OF A TRANSONIC M-WING AIRCRAFT

by

J. B. W. Edwards

SUMMARY

Free-flight tests have been made on a model of an M-wing aircraft designed to cruise at  $M = 1.2$  with a subsonic type of flow on the wing surfaces.

Results are presented for the zero-lift drag and longitudinal stability characteristics over the Mach number range from 0.9 to 1.3.

It is shown that the design aims have been achieved in that no evidence of shocks in the wing root was found and that some suppression of the wing wave drag occurred.

The results are compared with those from free-flight tests on a swept-wing model having the same body, fin and tailplane configuration.



CONTENTS

	<u>Page</u>
1 INTRODUCTION	4
2 DESCRIPTION OF THE MODELS	4
2.1 The M-wing models	4
2.2 The swept-wing model	6
3 FLIGHT DETAILS	6
4 DISCUSSION OF RESULTS	6
4.1 Pressure measurements	7
4.2 Zero-lift drag measurements	7
4.3 Comparison with swept-wing model	9
4.4 Lift and pitching moment derivatives	9
4.5 The damping derivatives	11
5 CONCLUSIONS	12
SYMBOLS	13
REFERENCES	14
APPENDIX 1 - Methods used in estimating the components of the zero-lift drag	16
TABLES 1-4	18-21
ILLUSTRATIONS - Figs.1-18	-
DETACHABLE ABSTRACT CARDS	-

TABLES

Table

1 Model data	18
2 Wing dimensions	19
3 Body ordinates	20
4 Nacelle ordinates	21

ILLUSTRATIONS

	<u>Fig.</u>
Arrangement of basic configuration (Model 2)	1
Arrangement of the preliminary model (Model 1)	2
Photographs of the models and boost system	3 a,b,c
Arrangement of the swept-wing model (From Ref.3)	4
Velocity	5
Mach number	6
Reynolds number per foot	7
Trim lift coefficient	8
Trim incidence	9
Induced drag coefficient	10
Measured drag coefficients	11(a) - (d)
Total drag coefficient	11a
Zero-lift drag of the wing-body-nacelles combination	11b
Wing-body-nacelles combination wave drag	11c
Wing-body-nacelles combination zero-lift wave drag factor, $K_0$	11d
Comparison of the wave drags of the M-wing and swept-wing models	12,a,b
Zero-lift wave drag, $C_{D_W}$	12a
Zero-lift wave drag factor, $K_0$	12b
Pitching-moment derivative $\frac{\partial C_m}{\partial \alpha}$ ( $\alpha = 0$ )	13
Manoeuvre margin	14
Lift-curve slope at zero incidence	15
Comparison between the stability derivatives of the M-wing and swept-wing models	16 (a) - (c)
Rotary damping-in-pitch - $[m_q + m_w]$	17
Total damping-in-pitch - $\left[ z_w + \frac{m_q + m_w}{i_B} \right]$	18

## 1 INTRODUCTION

A few years ago, studies undertaken by the Supersonic Transport Aircraft Committee of transatlantic aircraft showed that a case could be made for an aircraft designed to cruise at  $M = 1.2$  because values of the product of lift-to-drag ratio and Mach number could be achieved comparable with those obtained at subsonic speeds. Some suitable aerodynamic layouts for such aircraft were proposed by Bagley<sup>1</sup>. Two principal designs were put forward, the first a  $55^\circ$  sweptback planform of aspect ratio 3.4 and the second an M-wing layout of aspect ratio 5 with inner panels swept forward at  $55^\circ$  and the outer panels swept back at  $55^\circ$ . Both planforms had the same gross area.

A series of free-flight tests was undertaken to check some of the design principles involved. This note gives the first results from tests on a symmetrical M-wing model. There are a number of aspects in which the M-wing layout may have an advantage: it is possible to have a higher aspect ratio (5.0, say, instead of 3.4) and hence a lower drag-due-to-lift; it may be structurally preferable because of the elastic properties of the M-planform and because it can have a higher thickness/chord ratio; the smaller panels of the M-wing may give rise to thinner boundary layers near the trailing edge and hence the form drag as well as the control effectiveness may be better. One further advantage, not aerodynamic but nevertheless important, is that the required ground clearance of the wing tips can be achieved with a shorter undercarriage than for the swept-wing aircraft. A disadvantage of the M-wing layout is that the number of kinks in the planform is increased, and there is thus a need to take special steps to maintain the isobar sweep in the two additional kink regions. However, this can be done by adding bodies there and these can be used for engine nacelles or fuel tanks.

This note describes the results for zero-lift drag and longitudinal stability near zero lift, at Mach numbers between 0.9 and 1.3 for the first symmetrical M-wing model, together with a comparison with some of the results from free-flight tests on a corresponding symmetrical swept-wing model. Further work on the dynamic longitudinal stability at zero lift and at positive lift and on the drag-due-to-lift remains to be completed.

Complementary tunnel tests on the M-wing and swept-wing configurations were also initiated but only those on the swept-wing model have been completed<sup>10</sup>.

## 2 DESCRIPTION OF MODELS

### 2.1 The M-wing models

The M-wing planform chosen for these tests was of aspect ratio 5 with straight tapered inner panels swept forward at  $55^\circ$  on the quarter-chord line and having outer panels with straight trailing edges swept back at  $55^\circ$  and curved leading edges ending in streamwise tips (Fig.16, Ref.1). The uncambered aerofoil section was of 6% thickness/chord ratio and R.A.E.101 shape. Full details of the wing geometry are given in Table 2 and Fig.1.

The model was designed to have as far as possible, a comparable configuration to that of the swept-wing models<sup>2,3</sup>. The same scale was chosen giving a

wing area of 3.1 sq ft and an overall length of 80". The basic body shape was the same consisting of an ogival nose and tail with a cylindrical mid-body; the wings were set at zero incidence relative to the body. The body was waisted along the junction with the wing and was designed by Bagley's method<sup>4,5</sup> to give a pressure distribution in the junction at zero lift like that on the equivalent infinite sheared wing. The solid nacelles at the wing kinks half way along the span ( $\eta = 0.5$ ) were also waisted and the shapes were derived by the same method.

The effects of the nacelles on the wing-body flow and the effects of the body on the wing-nacelle flow were neglected in calculating either waisting. The body and nacelle ordinates are listed in Tables 3 and 4.

A fin and tailplane were added for experimental reasons and are not meant to be representative of the configuration investigated. They were identical to those used on the swept-wing model in order to give the same contributions to the drag and stability, apart from possible differences in downwash effects. Both fin and tailplane were of straight-tapered platform with the tailplane mounted on top of the fin. A general arrangement drawing of the basic configuration is given in Fig.1 and relevant model data in Table 1.

Two models of basically the same shape were flown. The first model (Model 1) was mainly intended to check on the performance of the boost-model combination, on the structural integrity of the model, and on the trim conditions. For economy, unwaisted body and nacelles were fitted and the after-body was cylindrical forming a blunt base since complete representation was not essential for these purposes. The forebody also was unrepresentative being a three-calibre ogive rather than a six-calibre ogive as on the basic design. The wings and tail assembly were, however, correctly represented. Model 1 was also fitted with pulse rockets to provide the disturbances necessary for the stability analysis. This model is illustrated by a general arrangement drawing in Fig.2. On the second model (Model 2) all the features to be investigated were represented.

The wings and tailplane, of both models, were manufactured by machining from solid aluminium alloy plate and were hand finished to a smooth surface with a tolerance on the ordinates of  $\pm 0.003$ ". Other components were finished to tolerances of  $\pm 0.005$ ".

Each model was fitted with a standard 465 Mc/s telemetry set radiating from a slot aerial in the fin trailing edge. Data were transmitted from accelerometers measuring the normal, lateral and longitudinal accelerations at the centre of gravity and normal accelerations at a forward and aft station. The second model carried thirteen pressure transducers to obtain the pressure distributions in the wing/body junction.

A photograph of both models and the boost-model combination is shown in Fig.3.

## 2.2 The swept-wing models

Since one of the objectives of these tests was to compare the performance of the M-wing models with the swept-wing models, a brief description of the latter is called for here; they are fully described in Refs.2 and 3. A general arrangement drawing of one of the free-flight models is given in Fig.4. The body and tailplane components are the same as for the M-wing models but the wing is of aspect ratio 3.4, with  $55^\circ$  of sweepback on the straight trailing edge. The leading edge is also straight and swept back at  $55^\circ$  up to the half span position; outboard of there, it is parabolic giving streamwise tips. The particular planform was proposed by Bagley in Ref.1. The position of the swept wing on the body is such that the leading edge of its aerodynamic mean chord,  $\bar{c}$ , is 41.58" aft of the nose whereas the M-wing is set with its leading edge of  $\bar{c}$  at 39.6" aft of the nose, a difference of some 2" or about 0.18  $\bar{c}$ . This has been allowed for when comparing the stability derivatives.

## 3 FLIGHT DETAILS

Each model was boosted to a maximum Mach number of about 1.3 by a solid-fuel rocket-motor assembly (Fig.3c). At burn out the model separated from the boost and continued in coasting flight while the measurements were made from which the results were analysed. Details of the range instrumentation and the methods of analysis are given in Ref.6. The velocity and Mach number records of both Models 1 and 2 are shown in Figs.5 and 6 and the Reynolds number per foot appropriate to these flight conditions is plotted against Mach number in Fig.7. Model 1 was flown at R.A.E. Larkhill and was destroyed after 10 seconds of flight for range safety considerations; Model 2 was flown at R.A.E. Aberporth and there was no need for a premature termination of the flight.

Model 1 was flown with its tailplane set at  $\frac{1}{2}^\circ$  positive incidence which successfully achieved the desired trim condition at zero lift; consequently the same tail setting angle was used on Model 2. However, the second model trimmed out at about +3g normal acceleration. This must have been caused by changed flow conditions over the tailplane, mainly resulting from the different after-body shape and perhaps by the waisting of body and nacelles. The corresponding lift coefficient is shown in Fig.8 and the trim incidence deduced from the trimmed lift coefficient and the measured lift-curve slope is shown in Fig.9. The trim incidence was about  $1.2^\circ$  at supersonic speeds, dropping to zero at sonic speed and rising again to over  $2^\circ$  subsonically. The significance of this trim on the zero-lift drag is discussed in Section 4.1.

The longitudinal stability derivatives have been obtained by the methods of Ref.6 for the bonker-excited oscillations of Model 1. Model 2 oscillated following the disturbance caused by separating from the boost and this oscillation has been analysed to give values at  $M = 1.3$  (Sections 4.2 and 4.3).

## 4 DISCUSSION OF RESULTS

Before discussing the results in detail it is desirable to outline the objectives of the tests rather more fully than in the Introduction. The design

principles involved are to maintain a subsonic type of flow over the wing surface, with no shock waves occurring on the wing and thus to obtain an adequate performance and flight behaviour. This is more difficult to achieve on an M-wing than a swept wing because of the additions of the extra kinks, but can be attempted by the use of nacelles at the kinks. The body shaping and nacelle design are aimed at maintaining in the junctions the subsonic type of flow that should occur over the remainder of the wing by virtue of its planform and section. Bagley<sup>1,5</sup> has explained such facets of the design in detail and in applying his methods the curvature of the body and the effects of body on nacelles and vice-versa have been ignored. Since it is not possible in free-flight to visualise the flow two methods are available for checking on the success of the design methods:- pressure measurements and drag measurements.

#### 4.1 Pressure measurements

Model 2 was fitted with pressure transducers measuring conditions in the wing-body junction on the upper surface of the wing. The construction of the model did not permit any measurements to be taken across other sections of the wing or at the nacelles. Those in the wing root partially failed so no results from them are given, but they did confirm one aspect of the effectiveness of the body waisting by showing a subsonic type of pressure distribution across the wing chord at  $M = 1.3$  downwards, i.e. there are no indications of shock waves on the wing root, but this does not necessarily imply that no shocks occur over other parts of the wing surface. The free-flight drag measurements and tunnel drag measurements on a similar M-wing model<sup>11</sup> suggests that a shock is occurring somewhere at  $M > 1.1$ . As the speed fell the pressure instruments gave increasingly untrustworthy results and this qualitative conclusion on the type of flow is the only one that can safely be drawn from them.

#### 4.2 Zero-lift drag measurements

The design method should eliminate the wave drag of the wing so a close examination and breakdown of the measured drag may well show how successful the design has been.

The measured drag of Model 2 is shown in Fig. 11a for the whole of the speed range,  $M = 0.85 - 1.3$ , covered by the test. These measurements were obtained from both longitudinal-accelerometer data and from velocity-time data given by kinetheodolites. Model 1, because of its blunter nose, cylindrical afterbody, unwaisted centrebody and nacelles and inferior surface finish had a much higher drag and was not sufficiently representative for its drag measurements to have any significance here and the results are not presented.

As mentioned in Section 3, Model 2 was not flown at zero lift; hence the measured drag is not quite the zero-lift drag value. Estimates of the induced drag factors of  $K_V = 1.2$  and  $K_W = 1.5$  have been assumed and the increment in drag  $\Delta C_{D_i}$  due to lift has been evaluated from the expression

$$\Delta C_{D_i} = \frac{K}{\pi A C_L^2}$$

where

$$K = K_V + K_W \beta^2 \left( \frac{S}{\ell} \right)^2 .$$

The variation of  $\Delta C_{D_i}$  is shown in Fig. 10 and is about 0.0005 at supersonic speeds, zero at  $M = 1$  and rises to 0.0011 at subsonic speeds. These corrections are necessarily only approximate but show the magnitude of the effect on  $C_D$  of the model flying at zero lift.

Since the design methods are only concerned here with the wing, body and nacelles in combination the zero-lift drag is re-presented in Fig. 11b as the measured drag minus the induced drag corrections from above and also with the fin and tailplane contributions to the drag subtracted; so the curve shown is thus the drag of the wing-body-nacelles combination. The contribution to this drag from skin friction is also shown, hence the difference represents the wave drag. The methods used for estimating the skin friction and the wave drags of the various components are given in detail in Appendix 1.

The subsonic drag level shown in Fig. 11b is rather higher than the estimated skin friction, indicating that there is a small amount of form drag present, perhaps from small separations in the waist of the body. The overall accuracy of the measurement of drag at subsonic speeds is poor, about  $\pm 12\%$ , and the skin friction estimates are dependent on the location of transition, hence no firm conclusion concerning form drag can be made.

To facilitate comparison of the wave drag with estimates the difference between the skin friction and the measured drag in Fig. 11b has been replotted in Fig. 11c which is thus the measured wave drag of the wing-body-nacelle combination\*. Ideally one would like to provide a theoretical estimate of this wave drag for comparison but the very unusual area distribution of the combination has prevented one being obtained, hence two alternative estimates which provide an upper and lower limit to the expected drag level have been obtained and are also shown in Fig. 11c. Details of the derivation of these estimates are given in the Appendix. The upper limit taken is the sum of the wave drags of the individual components treated in isolation and the lower limit is that of the optimum body of revolution of the same overall volume and length as the experimental configuration.

The measured drag lies between the two limits and shows that a very reasonable reduction in wave drag of the combination has been achieved from that of the isolated components. This reduction clearly suggests that the careful design of the body and nacelle waisting together with the choice of planform and section has created a low drag combination. The present design is probably not the best that can be obtained but it is doubtful whether a value approaching that of the equivalent Sears-Haack body is practicable whilst retaining other aerodynamic features of the design. Although the design Mach number was 1.2, it is clear that drag reductions occur at all the Mach numbers of the test, but as the Mach number increases the wave drag increases towards the value of the separate components.

The assessment of wave drag is now usually presented in terms of the wave drag factor  $K_o^{**}$  - the ratio of the wave drag of a configuration to that of its

\* A more usual approach is to present the difference between the measured subsonic and supersonic drag levels as the wave drag, but this has not been done because of the relatively high uncertainty in the measured subsonic drag level.

\*\*  $K_o = C_{D_W} \frac{\pi}{128} \frac{S \ell^4}{V^2}$  where  $C_{D_W}$  = wave drag coefficient,  $S$  = gross wing area,  $\ell$  = overall length,  $V$  = volume.

equivalent Sears-Haack body - so this has been done in Fig.11d where the measured value and the two theoretical "limits" are shown. The lower level by definition now is equal to unity. The measured drag factor is of the order of 2, which is reasonable for a complete configuration including nacelles. Slender wings designed for higher Mach numbers can have values of  $K_0$  less than one, but some proposed designs give values of 2 and above so the present design can be considered better than even some slender wings tested and thus a most satisfactory first attempt utilising the M-wing planform but one which leaves room for possible further improvements.

#### 4.3 Comparison with the swept-wing model

Several slightly different versions of the swept-wing model have been flown to investigate the effects on the drag of body waisting designed by a variety of methods<sup>3</sup>. Configuration 4 was the nearest in design to the waisting of the M-wing models and results from it are used here for comparison. Since the subsonic drag level was not established for the swept-wing models, the wave drags only are considered. In Fig.12a the wave drag of the swept-wing body combination is shown together with the M-wing results. The swept-wing results were obtained in a similar way to the M-wing results by subtracting the estimated skin-friction drag and fin and tailplane drag from the measured total drag. The M-wing values are roughly twice that of the swept wing and they show remarkably similar trends with Mach number. The M-wing results, of course, include the drag of the nacelles which probably accounts for much of the apparent difference; to illustrate this the wave drag of the isolated nacelles has been shown on the figure subtracted from the M-wing results. This isolated nacelle drag will not correspond to the drag of the nacelles as installed on the wing, but shows the order of magnitude of such drag. It is not known what the installed drag of similar nacelles on the swept-wing model would be; so it is not possible to say categorically that one is of lower drag than the other but the results shown in this figure suggest that only relatively small differences will exist.

The comparison is made again in Fig.12b in terms of  $K_0$ . A value calculated from linear theory for the swept-wing-body combination is also shown. Good agreement exists but a comparable theoretical value for the M-wing has not been worked out, as was mentioned in Section 4.2.

A further series of free-flight tests on the swept-wing models with nacelles is proceeding and more detailed comparison must await the results from them.

#### 4.4 Lift and pitching-moment derivatives

Measurements of the longitudinal stability derivatives of the model have been made to investigate the behaviour of the configuration as the Mach number varies through the transonic speed range, in particular the movement of the aerodynamic centre, which is useful for the evaluation of trim drag penalties associated with the M-wing planform. Also, comparison with the stability results from the swept-wing model is one of the objectives of the tests. If

the flow is as designed for, it should be possible to calculate some of these derivatives, but no such calculations have been made; the results discussed here are all experimental.

The methods of analysis used to obtain the stability derivatives are given in detail in Ref.6 but each method used is outlined briefly here.

The pitching-moment derivatives,  $\partial C_M / \partial \alpha$ , comes directly from the frequency of the short-period longitudinal oscillation of the model following a disturbance. Results have been obtained at five Mach numbers for Model 1 from the pulse-rocket-induced oscillations and at the maximum Mach number only for Model 2 from its separation oscillation; these are shown in Fig.13. Since the magnitude of this derivative depends on the centre of gravity position, the results have been adjusted to a common G.C. position of 40.5" aft of the nose. This pitching moment varies only slightly with Mach number and the agreement between the results for Models 1 and 2 is good considering the geometrical differences which exist between them.

The manoeuvre margin, based on the aerodynamic mean chord,  $\bar{c}$ , was derived by the focal-point method using the pitching acceleration obtained from longitudinally displaced accelerometers. This is a somewhat less accurate measurement than the pitching-moment derivative; it is typically accurate to  $\pm 6\%$ . The results are shown in Fig.14 and the somewhat higher value for Model 2 is probably a real effect introduced by the nacelle and body waisting and the different afterbody shape. The increase in manoeuvre margin at supersonic speeds must be caused by a decrease in the lift-curve slope since  $\partial C_M / \partial \alpha$  did not show any such sudden increase.

The lift-curve slope,  $\partial C_L / \partial \alpha$ , was obtained from the manoeuvre margin and  $\partial C_M / \partial \alpha$  by neglecting the term  $Z_w m_q$  compared with the term  $\mu_1 m_w$ , which is justified because  $\mu_1$ , the relative density, for a free-flight model is large - in this case 575 - whereas the other terms are all of order unity. Hence the values deduced for  $\partial C_L / \partial \alpha$  are an excellent approximation to the true value. The results are shown in Fig.15.

The trend with Mach number is very similar to that measured in tunnel tests<sup>11</sup> on a slightly different M-wing model, which had a peak in  $\partial C_L / \partial \alpha$  of 4.5 at transonic speeds and a value of 3.7 at low supersonic speeds.

On the tunnel model the peak occurred at  $M = 0.97$  whereas the present results showed a peak at  $M = 1.1$ .

Since no calculated values have been obtained for these derivatives a simple comparison with similar results from the swept-wing model test<sup>2</sup> has been made. These comparisons are shown in Fig.16a,b,c. Both sets of results have been corrected to a moment reference centre at the aerodynamic mean  $\frac{1}{4}$ -chord point in order to eliminate the effect of wing position on the body. These points are M-wing;  $\frac{1}{4} \bar{c} = 42.31$ " aft of nose: swept-wing;  $\frac{1}{4} \bar{c} = 44.53$ " aft nose. The reference point in Fig.13 and 14 was 40.5" aft nose hence the pitching-moment derivative and manoeuvre margin are reduced in Fig.16a and b.

Consider first the lift-curve slope,  $\partial C_L / \partial \alpha$  (Fig.16c). The swept-wing value varies only slowly with Mach number and is lower than the M-wing throughout. The higher aspect ratio of the M-wing (5 compared to 3.4) is expected to give a higher value of  $\partial C_L / \partial \alpha$ , but the difference between the measurements, particularly at supersonic speeds, does not appear as great as might be expected. It is not known why this is so, but is possible for the composite planforms, such as that of an M-wing, that the effective aspect ratio may be closer to the aspect ratios of the separate panels than to that of the whole wing. The nacelles on the M-wing will contribute to the lift and may be responsible for the peak in the curve at  $M = 1.1$ .

The pitching-moment derivatives,  $\partial C_M / \partial \alpha$ , and the manoeuvre margin (Figs.16a and b) closely show that the swept-wing model was considerably more stable, i.e. it developed its lift further aft than the M-wing, and that the swept-wing exhibits a much greater rearward shift of aerodynamic centre position with increasing Mach number than the M-wing. The first point is not of great significance since the wing position on the body is at the choice of the designer, but the shift in aerodynamic centre is much more important. If an aircraft is balanced for minimum trim drag during the cruise a large shift in aerodynamic centre between subsonic and cruise conditions will result in a large trim drag during subsonic operation. This feature could represent an important advantage for the M-wing design if this trend is confirmed from the further tests that are planned on the basic design model: remembering that the majority of the present stability results are from the unwaisted Model 1.

#### 4.5 The damping derivatives

The total damping-in-pitch,  $- \left[ Z_w + \frac{m_q + m_w}{i_B} \right]$ , and the rotary component of this damping ( $m_q + m_w$ ) are shown in Figs.17 and 18. The total damping is derived directly from the measured decay of the longitudinal short-period oscillations, and the rotary component is then deduced using the measured values of  $Z_w$  ( $\approx \frac{1}{2} \partial C_L / \partial \alpha$ ) and the inertia coefficient,  $i_B$ .

The total damping decreases slowly with increasing Mach number and shows no sudden changes over the transonic speed range. The agreement between Models 1 and 2 is reasonable and the general level suggests that there is adequate damping at all speeds.

The rotary component of the damping ( $m_q + m_w$ ) does not show such a smooth variation but this dip in the curve is a reflection of the peak in  $\partial C_L / \partial \alpha$  (Fig.14). The agreement with Model 2 is still very close.

For comparison, the swept-wing model results<sup>2</sup> are also shown on the figure. The curves have not been corrected to a common centre of gravity position, since such a correction involves varying derivatives not measured in the experiment, and will in any case be small.

The fact that total dampings are very much the same in both cases is purely fortuitous because there were large differences in the inertia

coefficient  $i_{\beta}$  between the two models, 1.6 for the swept wing models against 3.2 for the M-wing model. The rotary damping,  $m_{\dot{\alpha}} + m_{\dot{\omega}}$ , showed large differences in magnitude and variation with Mach numbers but the general damping characteristics appear satisfactory for both configurations.

## 5 CONCLUSIONS

Free-flight tests have been made on two models of an M-wing aircraft configuration, designed to maintain a subsonic type of flow over the wing surfaces with no shock waves occurring on the wings, at speeds up to a Mach number of 1.3.

Results on the longitudinal stability of the configuration have been obtained from a simplified preliminary model and measurements of the total drag and the wing root pressure distribution were made on a second fully representative model. From these latter results it has proved possible to deduce that the design principles have been achieved. Comparisons with results from free-flight tests on a swept-wing configuration designed in a similar way have been made. The main conclusions are:-

- (1) The pressure measurements in the wing root, although partially unsuccessful, were adequate to show at the highest Mach numbers that a subsonic type of flow was established there and that no evidence of shock waves existed.
- (2) The zero-lift wave drag of the wing-body-nacelle combination has been evaluated from the measured total drag by subtracting the contributions from skin friction and the fin and tailplane, and is shown to be lower than that of the sum of the wave drags of the components in isolation. This indicates that some suppression of the wing wave drag expected from the design has occurred. It is not possible to calculate the body and nacelle drag as installed; so one cannot deduce whether all the wing wave drag was suppressed.
- (3) The wave drag factor  $K_D$  is 2.4 at the design Mach number of 1.2. This is considered reasonably low for a first attempt at such a configuration. It is roughly twice that of a comparable swept-wing-body combination but the contribution from the nacelles that are included in the M-wing drag factor is probably responsible for the major part of this increase.
- (4) The M-wing model has a somewhat higher lift-curve slope than the swept-wing model owing to its higher aspect ratio. The shift in aerodynamic centre position through transonic speeds was about  $0.1 \bar{c}$  compared with  $0.2 \bar{c}$  for the swept-wing model. If subsequent tests confirm this latter result the easing of the problem of trimming that it implies could prove to be an important additional advantage of the M-wing design.
- (5) No undesirable damping characteristics in the damping-in-pitch were observed between  $M = 0.95 - 1.3$ .

SYMBOLS

- A aspect ratio
- B moment of inertia about y-axis (slug ft<sup>2</sup>)
- b gross wing span (ft)
- C<sub>D</sub> drag coefficient: suffices, o, at zero lift, w, wave, i, induced
- C<sub>L</sub> lift coefficient
- C<sub>m</sub> pitching moment coefficient
- C<sub>z</sub> normal force coefficient
- c local chord at station y (ft)
- $\bar{c}$  aerodynamic mean chord (ft)
- g acceleration due to gravity (ft/sec<sup>2</sup>)
- i<sub>B</sub>  $\frac{Bg}{W\bar{c}^2}$  . inertia coefficient
- K induced drag factor (defined in Section 4.2)
- K<sub>o</sub> wave drag factor (see footnote to page 8)
- M Mach number
- m<sub>q</sub>  $\frac{1}{2} \frac{\partial C_m}{\partial \left( \frac{q\bar{c}}{V} \right)}$
- m<sub>v</sub>  $\frac{1}{2} \frac{\partial C_m}{\partial \left( \frac{q\bar{c}}{V^2} \right)}$
- q angular velocity about y-axis (rad/sec)
- S gross wing area (sq ft)
- v velocity along flight path (ft/sec)
- W weight (lb)
- $\dot{w}$  acceleration along the z-axis (ft/sec<sup>2</sup>)

SYMBOLS (Contd.)

- $x, y, z$  Cartesian co-ordinates referred to axes fixed in the model, passing through its C.G. (x-axis along centre-line, y-axis lateral, z-axis normal)
- $Z_w$   $-\frac{1}{2} \frac{\partial C_z}{\partial \left(\frac{w}{V}\right)}$
- $\alpha$  angle of incidence
- $\beta$   $\sqrt{M^2 - 1}$
- $\eta$   $\frac{y}{b/2}$
- $\rho$  air density (slug/ft<sup>3</sup>)

REFERENCES

<u>No.</u>	<u>Author(s)</u>	<u>Title, etc.</u>
1	Bagley, J.A.	An aerodynamic outline of a transonic transport aeroplane. ARC.19205 Oct. 1956.
2	Hunt, G.K.	Free-flight measurements at transonic speeds of the dynamic longitudinal stability of a transonic swept-wing aircraft. Unpublished M.O.A. Report.
3	Hunt, G.K.	A free-flight investigation of wing-body junction design for a transonic swept-wing aircraft. A.R.C. C.P. 759. August, 1963.
4	Küchemann, D. Hartley, D.E.	The design of swept wings and wing-body combinations to have low drag at transonic speeds. ARC 17869. April 1955.
5	Bagley, J.A.	Some aerodynamic principles for the design of swept wings. Progress in Aeronautical Science, Vol.3, Pergamon Press 1962.
6	Hamilton, J.A. Hufton, P.	Journal of Royal Aeronautical Society. March 1956.
7	-	R.Ae.S. Data Sheets S.02.04.12.
8	Weber, J. Brebner, G.G.	A simple estimate of the profile drag of swept wings. A.R.C. 15 246. June, 1952.

REFERENCES (Contd.)

<u>No.</u>	<u>Author(s)</u>	<u>Title, etc.</u>
9	Bishop, R.A. Cane, E.G.	Charts of theoretical wave drag of wings at zero-lift. A.R.C. C.P.313. June, 1956.
10	Haines, A.B. Jones, J.C.M.	Transonic Tunnel Tests on a 6% thick, warped 55° swept- back wing model. Aircraft Research Assoc. Wind Tunnel Note 25. C.R.A.G. No.133 Sept.1960.
11	Haines, A.B.	Aircraft Research Association: Unpublished Communication. Oct. 1962.
12	Eminton, E.	On the minimisation and numerical evaluation of wave drag. A.R.C. 19212 Nov. 1955.

---

## APPENDIX 1

### METHODS FOR ESTIMATING THE VARIOUS COMPONENTS OF THE ZERO-LIFT DRAG

#### 1 SKIN-FRICTION DRAG

##### 1.1 Wing

The wing friction drag was calculated from the charts of Ref.7, assuming that transition occurred at the leading edge, which is considered most likely on a wing of high sweepback ( $55^\circ$ ) at the test Reynolds numbers (Fig.7). It has been suggested<sup>8</sup> that sweepback produces a reduction in skin friction. Estimates were made with and without this correction being applied. Heat-transfer conditions appropriate to the wall at ambient temperature were assumed to apply for all skin-friction estimates since the model is built largely of metals of high thermal conductivity and heat capacity. This assumption should not introduce any significant errors as the maximum speed was only 1400 ft/sec and the flight time was less than 30 seconds.

##### 1.2 Body and nacelles

Their friction drag was computed<sup>7</sup> for the exact wetted areas assuming transition occurred at a Reynolds number of 10 million on the body and at the wing root leading edge on the nacelles.

##### 1.3 Fin and tailplane

The friction drag was estimated with and without sweepback corrections, again using Ref.7, assuming transition occurred at the maximum thickness point on the tailplane and at the forward ridge line of the fin which was of trapezoidal section.

The extent of the sweepback corrections to the skin-friction components is shown in Fig.11a, but in subsequent deductions of the wave drag by subtraction of the skin-friction from the measured total drag they have not been applied. This is supported by transonic tunnel tests on one of the swept-wing free-flight models<sup>10</sup>, in which no evidence of this sweep effect was found.

#### 2 WAVE DRAG

##### 2.1 Wing, body and nacelles

The wave drags of the body and nacelles can be estimated by linear theory methods if they can be considered as separate bodies in isolation and this has been done but it is unrealistic to assume that the resulting drag can be considered as that of the body and nacelles in the presence of the wing since the design of the waisting of these components is totally dependent on the presence of the wing.

Present theoretical methods are not adequate to provide an estimate of the wave drag of the whole combination of wing body and nacelles which can be

## Appendix 1

compared with the measured wave drag. Two alternative approaches have been used in an attempt to provide a scale by which to judge the measured wave drag. The first was to calculate the wave drag of the equivalent optimum Sears-Haack body by assuming such a body was of the same volume and length as the wing-body-nacelle combination. The second method consisted of calculating the linear theory wave drags<sup>12</sup> of each component - wing, body and nacelles - considered in isolation and merely summing them. This should provide an upper limit to the measured wave drag which would only be attained if the design methods had failed to effect any reduction in the wing wave drag. It should be emphasised that neither of these two estimates are expected to be representative of the actual wave drag of the combination.

### 2.2 Fin and tailplane

The fin and tailplane wave drags were estimated using the charts of Ref.9 factoring the results to take account of the different sections of these components, since the charts are for double wedge sections.

TABLE 1

Model data

Aspect ratio	5	
Gross wing area	3.1 sq ft	
Nett wing area	2.55 sq ft	
Wing section	R.A.E. 101	6% t/c
Geometric mean chord $\bar{c}$	0.787 ft	
Aerodynamic mean chord $\bar{c}_a$	0.904 ft	
Tailplane aspect ratio	2.4	
Tailplane area	0.651 sq ft	
Tailplane section	Trapezoidal	4% t/c (mean)
Fin aspect ratio	0.6	
Fin area	0.736 sq ft	
Fin section	Trapezoidal	5.5% t/c (mean)
Body fineness ratio	16	
Body frontal area	0.136 sq ft	
	<u>Model 1</u>	<u>Model 2</u>
Weight	118 lb	111 lb
C.G. position, inches aft of nose	39.395	40.4
Inertia coefficient $i_B$ based on $\bar{c}$	3.249	2.620

TABLE 2

Wing dimensions

The curved leading edge of the outboard section of the wing is defined by the wing chord which is given by

$$\frac{c}{b/2} = 0.64 \{ \sqrt{2(1-\eta)} - (1-\eta) \} \quad \text{for } 0.5 < \eta < 1.0$$

where

$$\eta = \frac{y}{b/2} \quad . \quad y \text{ is the spanwise co-ordinate .}$$

The values of this expression are tabulated below.

$\eta$	Outer wing chord inches.
0.50	7.565
0.55	7.550
0.60	7.474
0.65	7.368
0.70	7.187
0.75	6.914
0.80	6.551
0.825	6.309
0.85	6.022
0.875	5.674
0.90	5.250
0.92	4.842
0.94	4.327
0.96	3.676
0.98	2.723
1.00	0

- Inner wing leading edge sweepback       $-50^{\circ} 36'$
- Inner wing trailing edge sweepback       $-64^{\circ} 5'$
- Inner wing quarter chord line  
sweepback       $-55^{\circ}$
- Outer wing trailing edge sweepback       $+55^{\circ}$

TABLE 3

Body ordinates (length = 80 in.)

Distance aft nose Inches	Body radius Inches (circular sections)	Distance forward base Inches
0	0	-
1	0.266	-
2	0.446	-
2.340	0.500	0
3	0.600	0.660
4	0.740	1.660
5	0.870	2.660
6	0.991	3.660
7	1.105	4.660
8	1.214	5.660
9	1.317	6.660
10	1.416	7.660
11	1.510	8.660
12	1.600	9.660
13	1.686	10.660
14	1.768	11.660
15	1.846	12.660
16	1.921	13.660
17	1.993	14.660
18	2.060	15.660
19	2.125	16.660
20	2.186	17.660
21	2.242	18.660
22	2.295	19.660
23	2.344	20.660
24	2.388	21.660
25	2.427	22.660
26	2.460	23.660
27	2.486	-
28	2.500	-
36.297	2.500	-
Elliptic sections		
	Plan ordinates	Elevation ordinates
37.837	2.442	2.500
39.376	2.331	2.500
40.916	2.188	2.500
42.455	2.001	2.500
43.985	1.907	2.500
43.994	1.907	2.500
45.534	1.965	2.500
47.073	2.056	2.500
48.613	2.164	2.500
50.152	2.267	2.500
51.691	2.366	2.500
53.231	2.442	2.500
54.755	2.478	2.497

TABLE 4.

NACELLE ORDINATES

The nacelle is symmetrical about its horizontal mid plane and its cross sections are elliptical but because the waisting profile is slightly different along the inboard and outboard junctions the cross sections over the wing chord are formed by two semi-ellipses sharing a common major axis but having different minor axes.

x in. aft nose	Plan ordinates		Elevation ordinates z
	y inboard	y outboard	
1.318	0.222	0.222	0.381
2.635	0.366	0.366	0.630
3.953	0.487	0.487	0.839
4.995	0.572	0.572	0.988
6.995	0.714	0.714	1.230
8.995	0.827	0.827	1.424
10.995	0.916	0.916	1.577
11.995	0.949	0.949	1.632
12.995	0.970	0.970	1.666
13.174	0.969	0.969	1.669
13.393	0.963	0.969	1.669
13.995	0.924	0.938	1.669
15.995	0.708	0.723	1.669
16.995	0.606	0.626	1.645
17.995	0.538	0.563	1.594
18.995	0.508	0.545	1.525
19.995	0.527	0.574	1.447
20.995	0.571	0.600	1.356
21.995	0.596	0.613	1.255
22.995	0.616	0.616	1.144
23.231	0.615	0.615	1.109
23.648	0.590	0.590	1.064
23.995	0.531	0.531	1.020
24.995	0.171	0.171	0.889
25.317	0	0	0.839



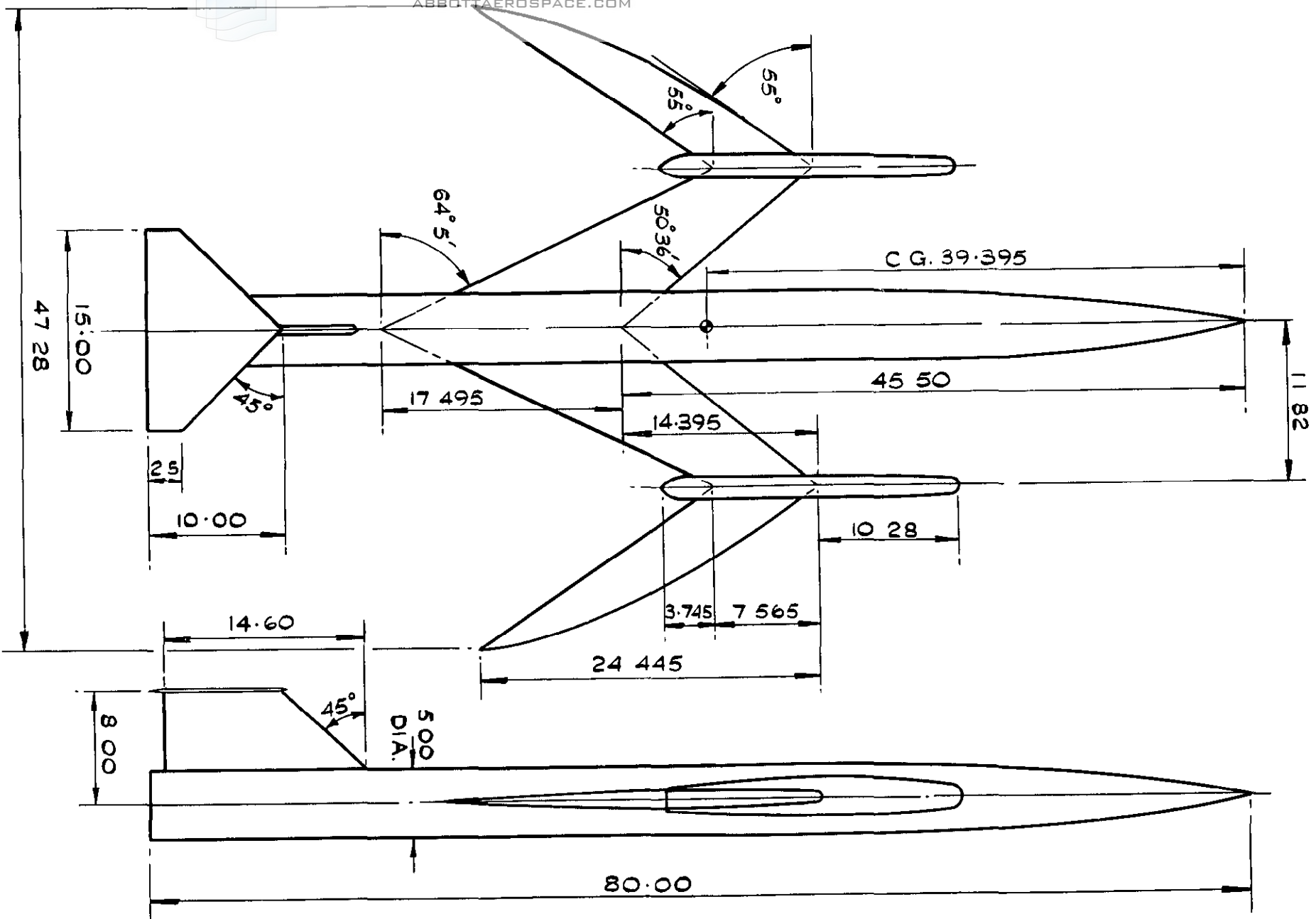
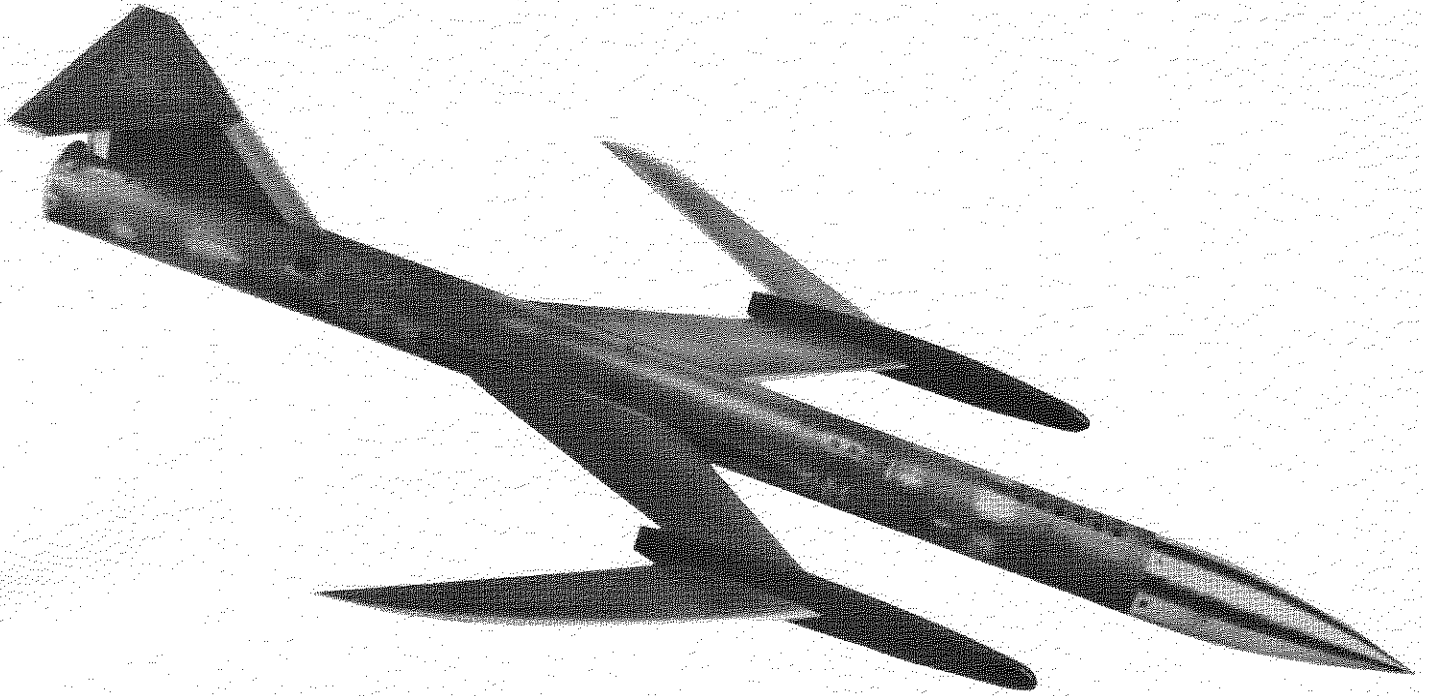
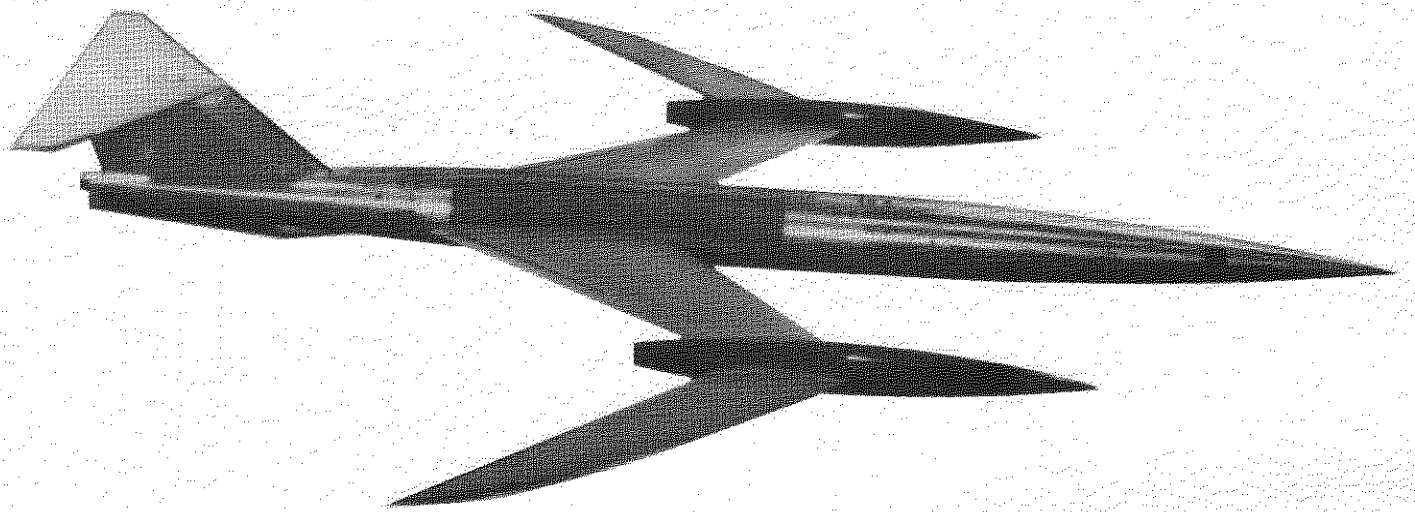


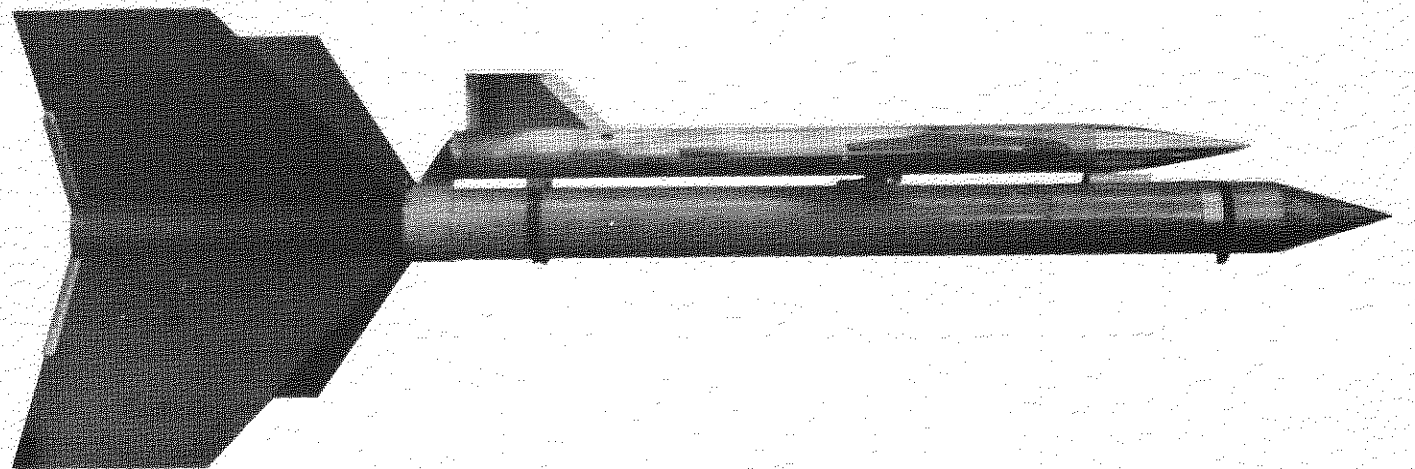
FIG. 2. GEN. ARR'GT. OF THE PRELIMINARY MODEL.  
MODEL I.



a. PRELIMINARY MODEL (STABILITY) MODEL 1



b. DRAG MODEL - MODEL 2



c. MODEL 1 MOUNTED ON BOOSTER

FIG.3a, b, & c. MODELS AND BOOSTER

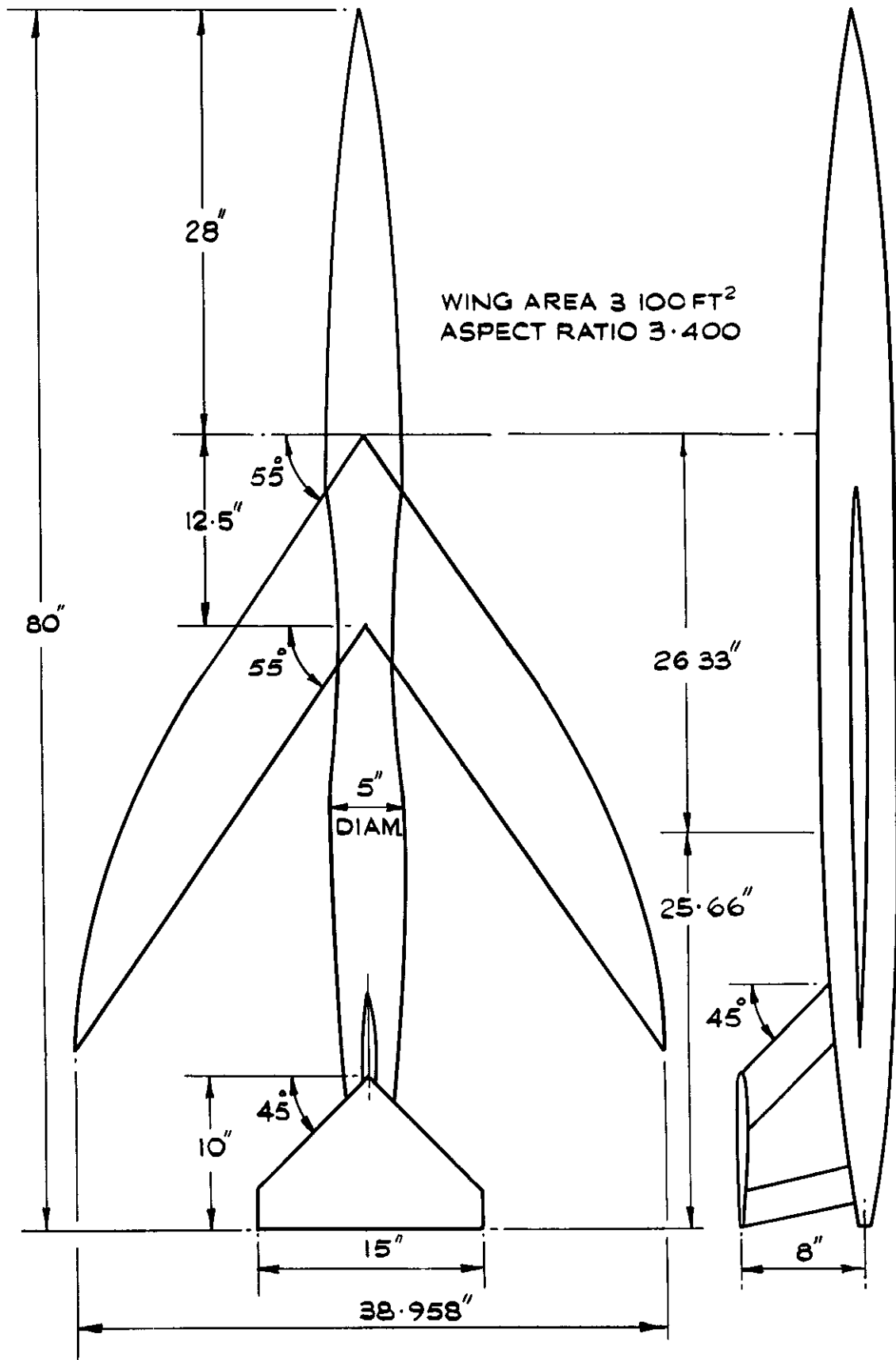


FIG.4. GENERAL ARRANGEMENT OF THE SWEEP-WING MODEL.  
(FROM REF.3.)

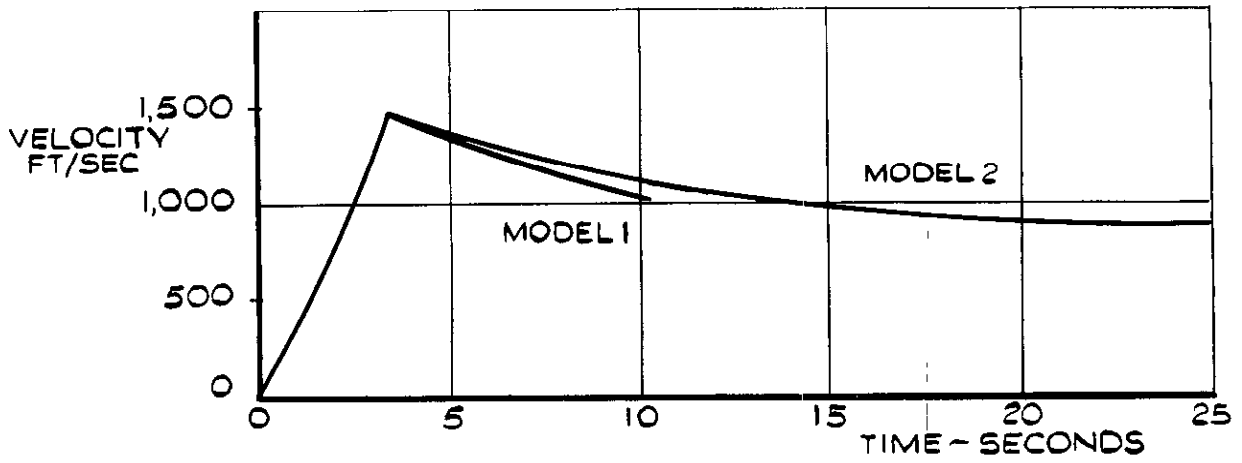


FIG. 5. VELOCITY.

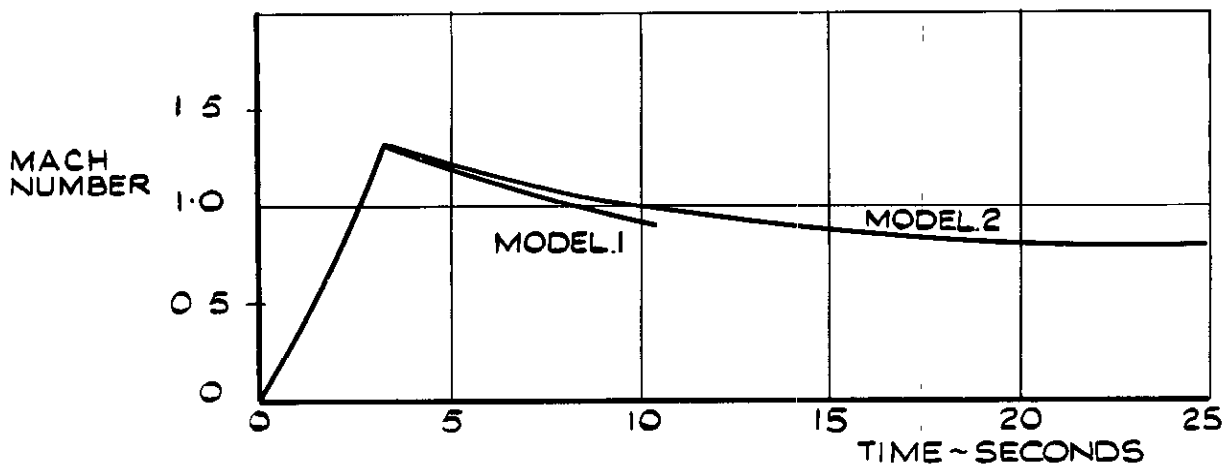


FIG. 6. MACH NUMBER.

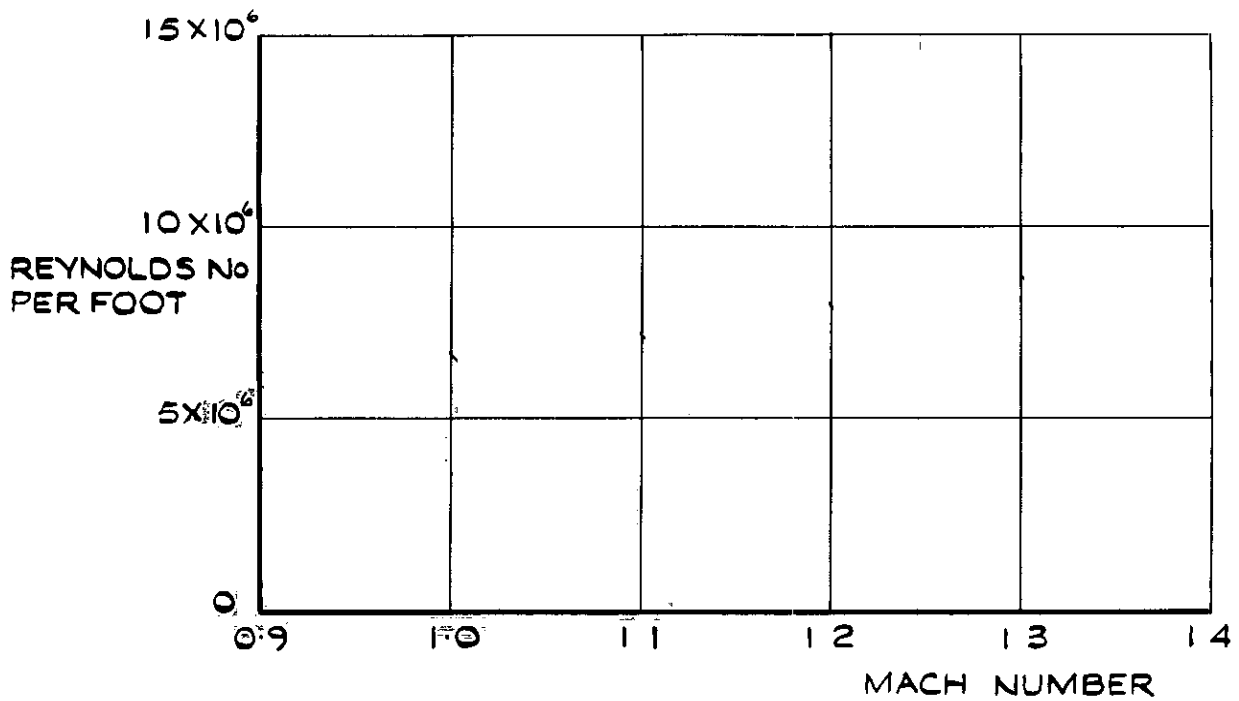


FIG. 7. REYNOLDS NUMBER PER FOOT.

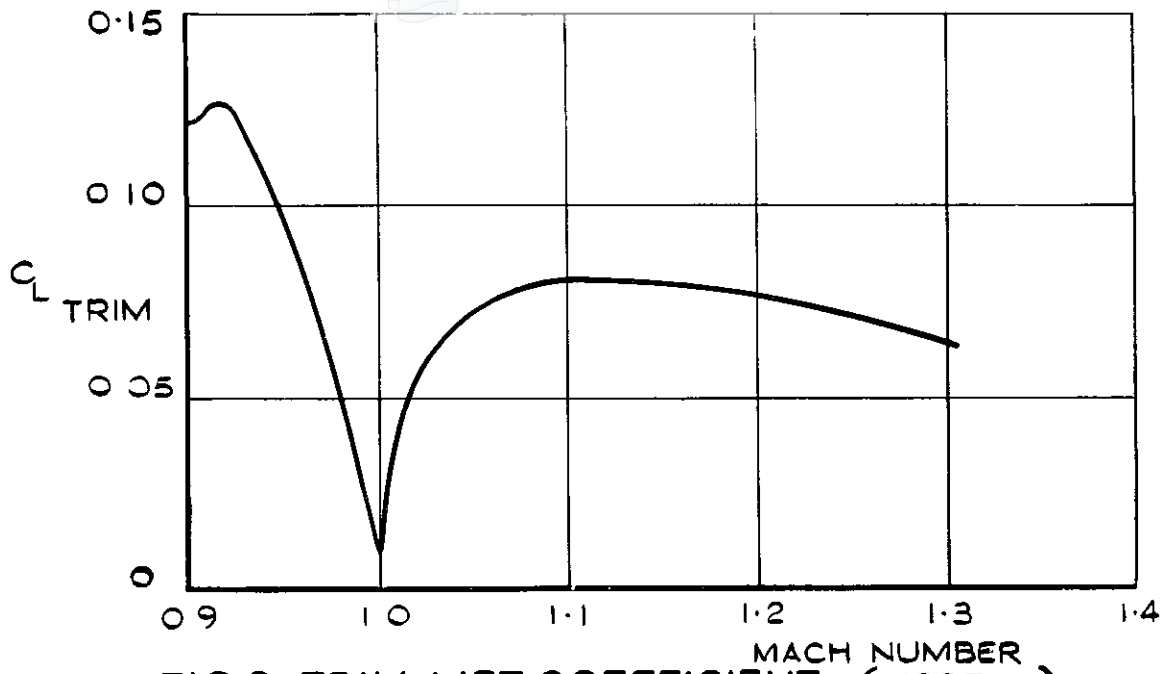


FIG.8. TRIM LIFT COEFFICIENT. (MODEL 2)

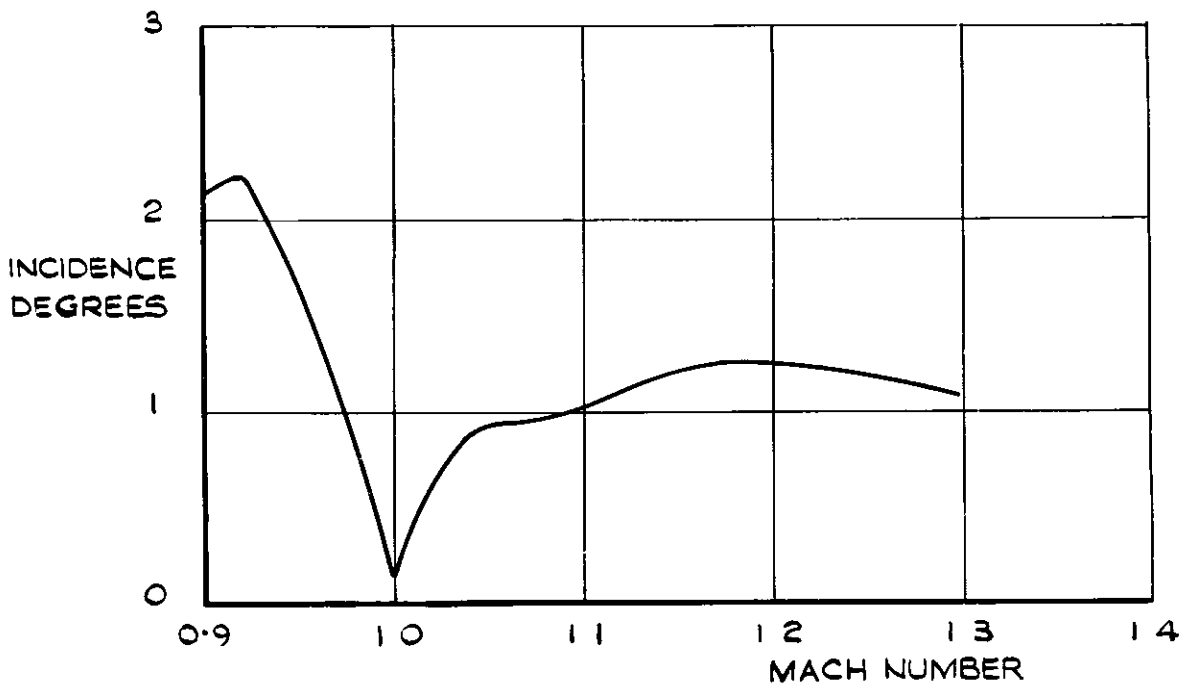


FIG.9. TRIM INCIDENCE. (MODEL.2)

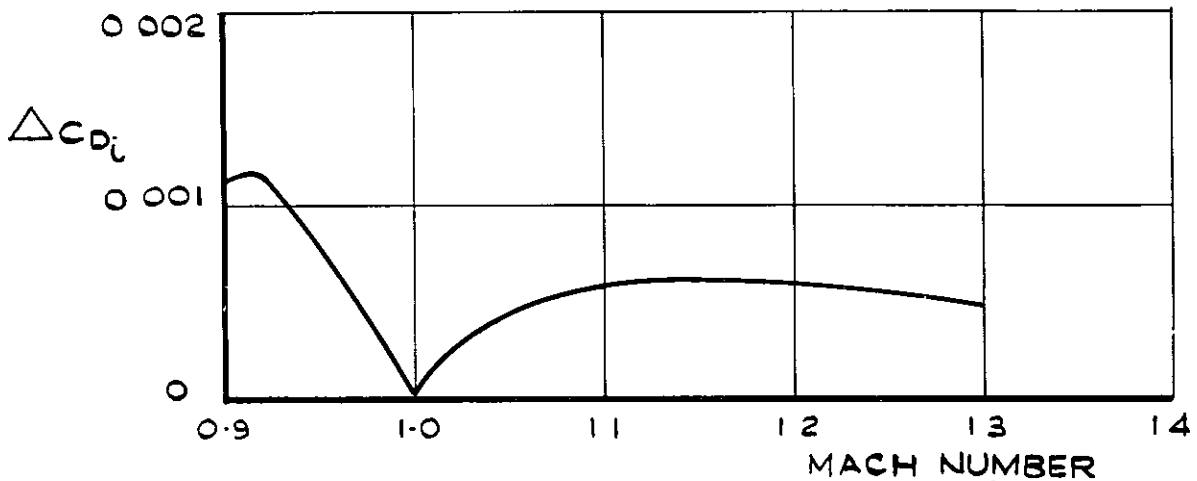
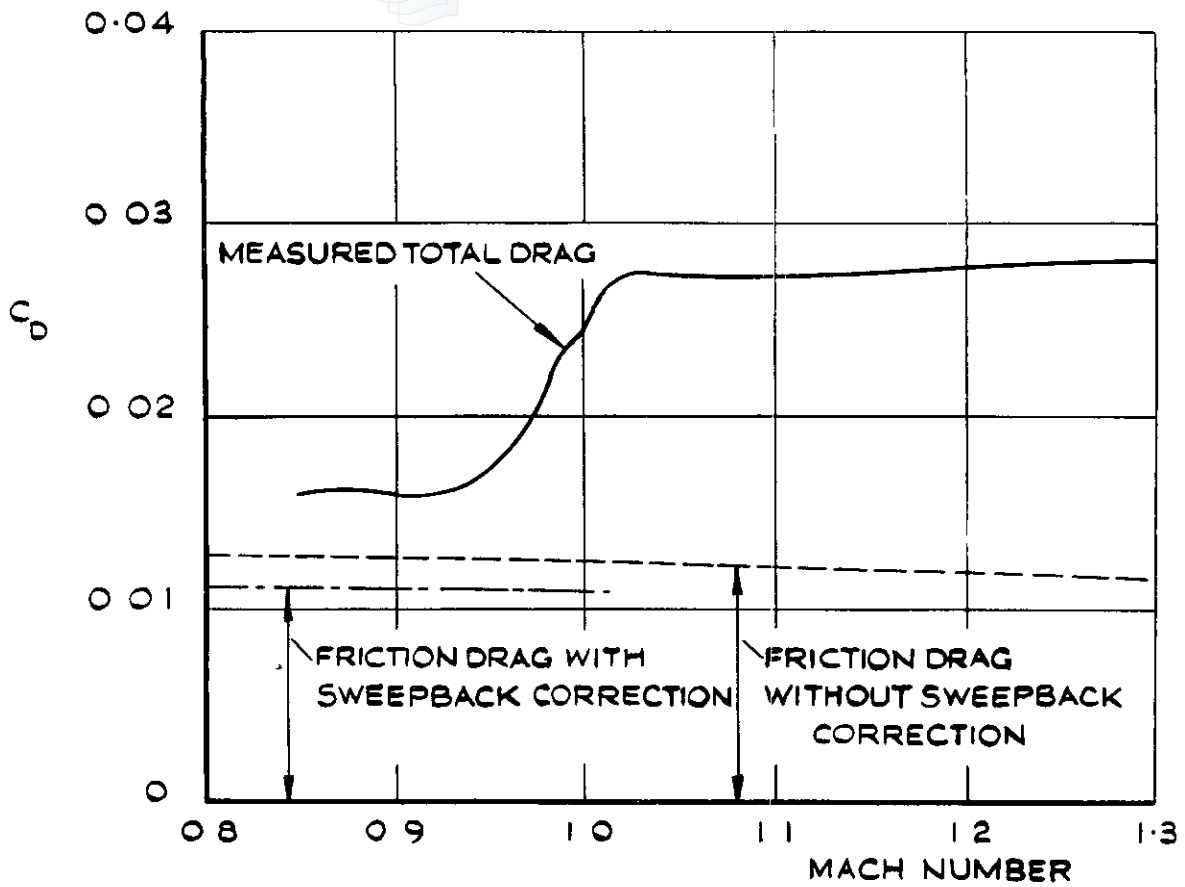
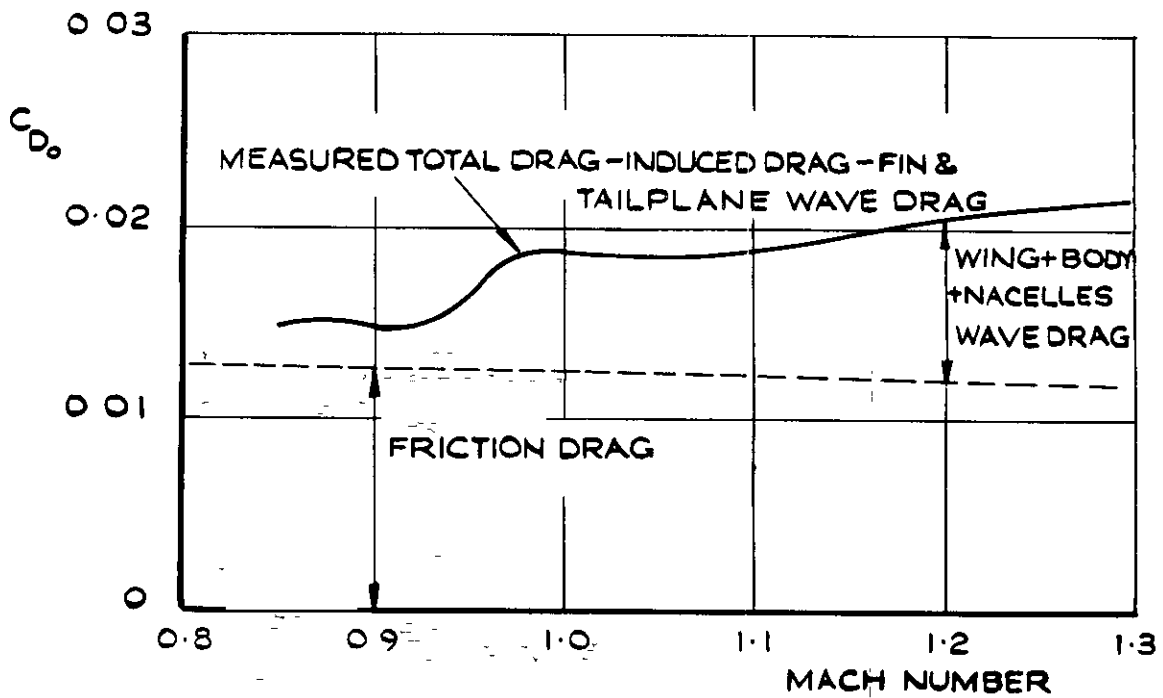


FIG.10. INDUCED DRAG COEFFICIENT. (MODEL.2)

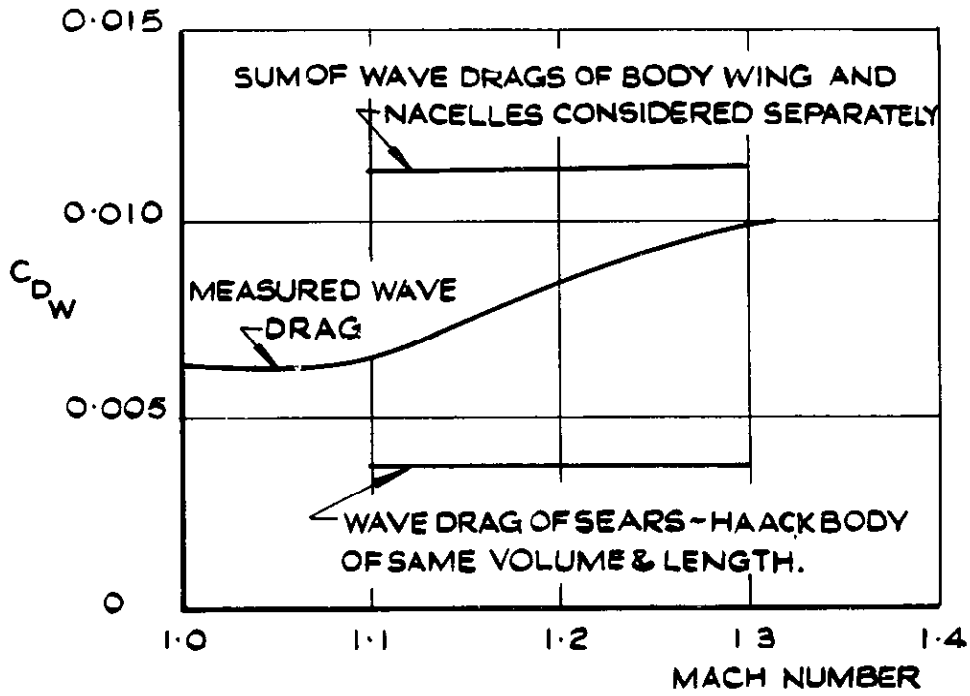


(d) MEASURED TOTAL DRAG COEFFICIENT

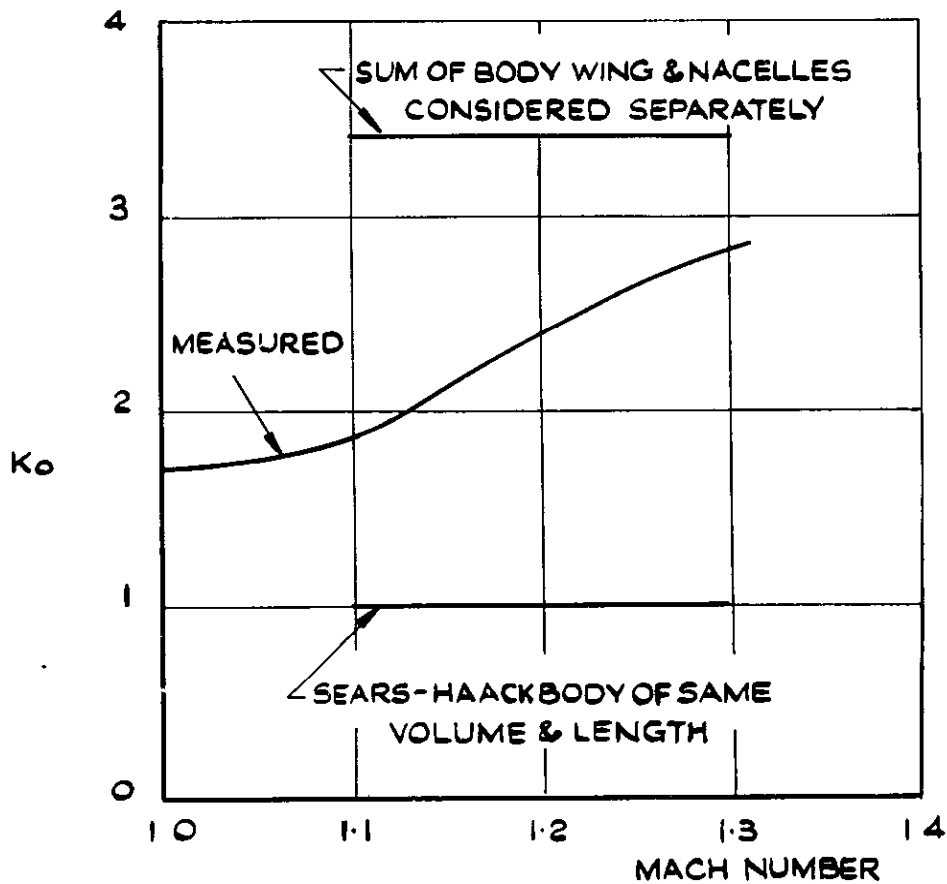


(b) ZERO-LIFT DRAG OF THE WING-BODY NACELLES COMBINATION.

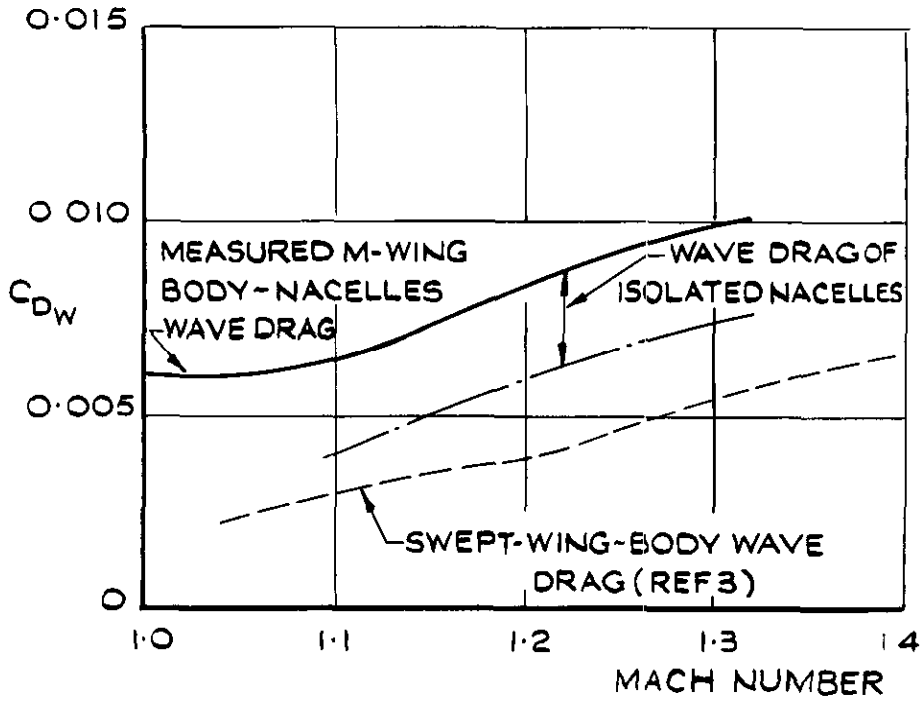
FIG.11. (a)-(d) MEASURED DRAG COEFFICIENTS.



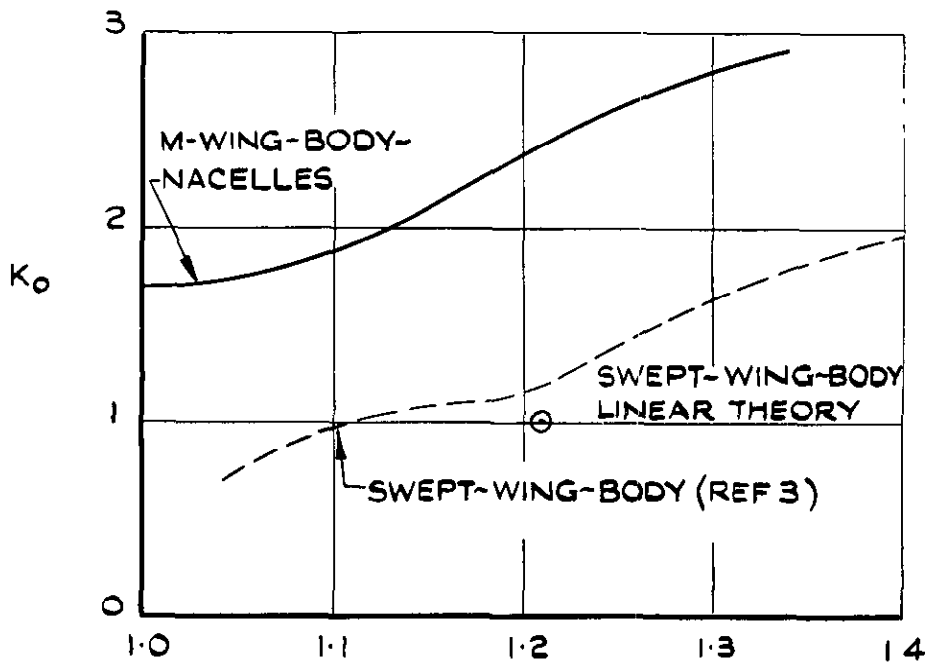
(c) WING-BODY-NACELLE COMBINATION WAVE DRAG.



(d) ZERO-LIFT WAVE DRAG FACTOR  $K_0$  FOR THE WING-BODY-NACELLES COMBINATION.



(a) ZERO-LIFT WAVE DRAG.



(b) ZERO-LIFT WAVE DRAG FACTOR  $K_0$ .

FIG.12.(a)(b) COMPARISON OF THE WAVE DRAGS OF THE M-WING & SWEPT WING MODELS.

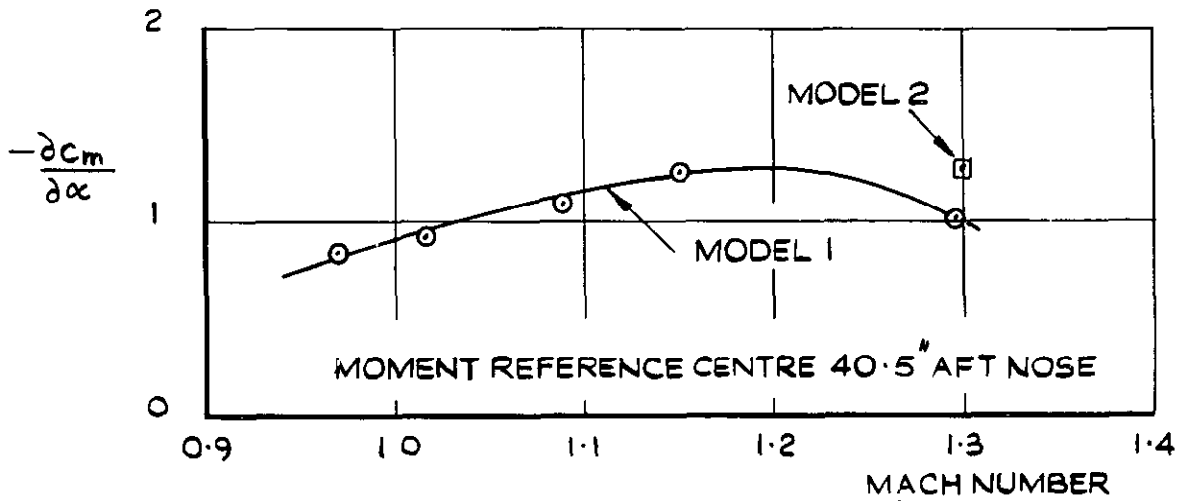


FIG.13. PITCHING-MOMENT DERIVATIVE  $\frac{\partial C_m}{\partial \alpha}$  ( $\alpha = 0$ )

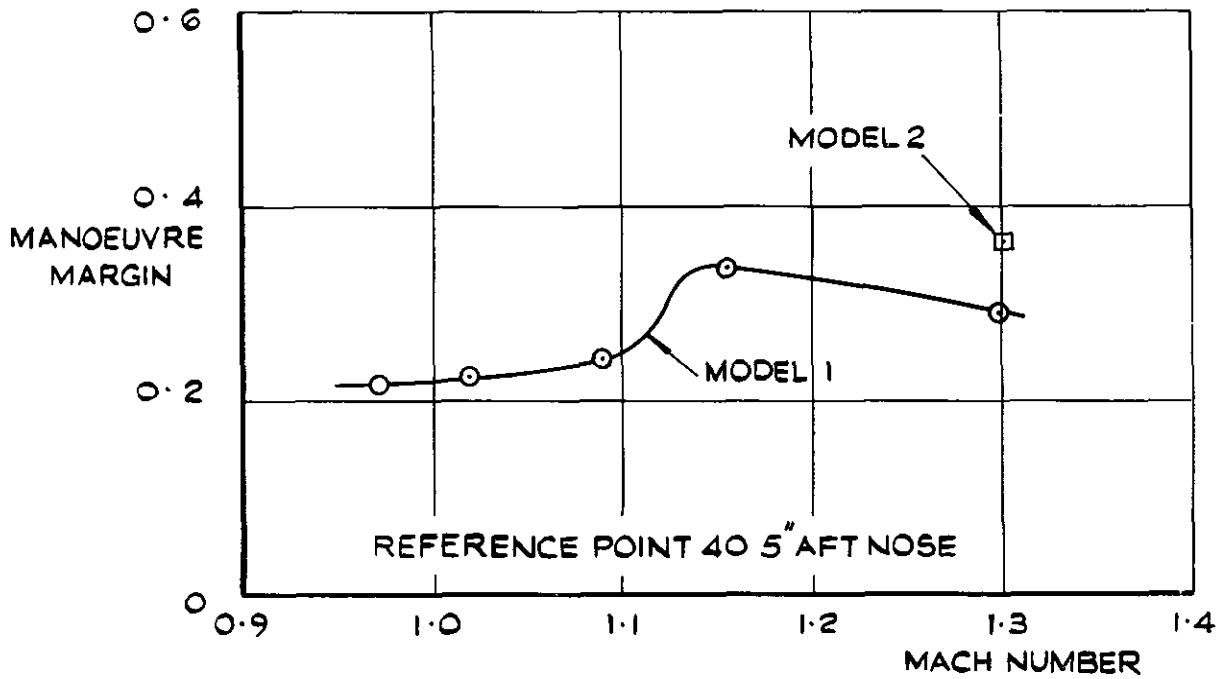


FIG.14. MANOEUVRE MARGIN.

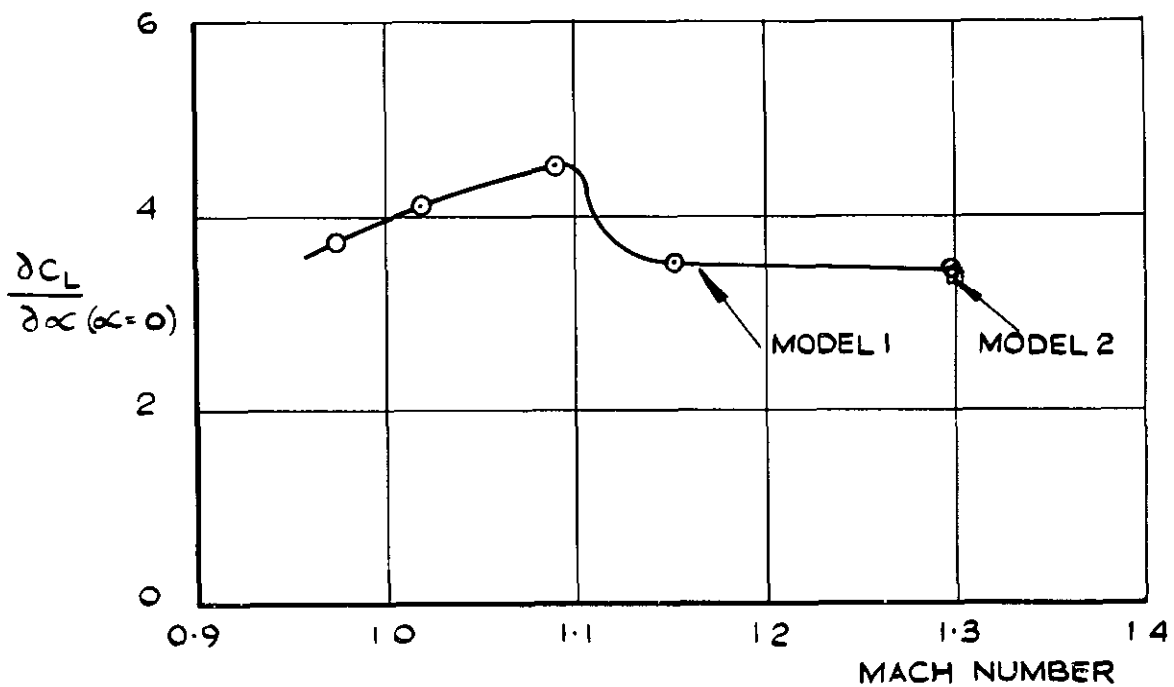
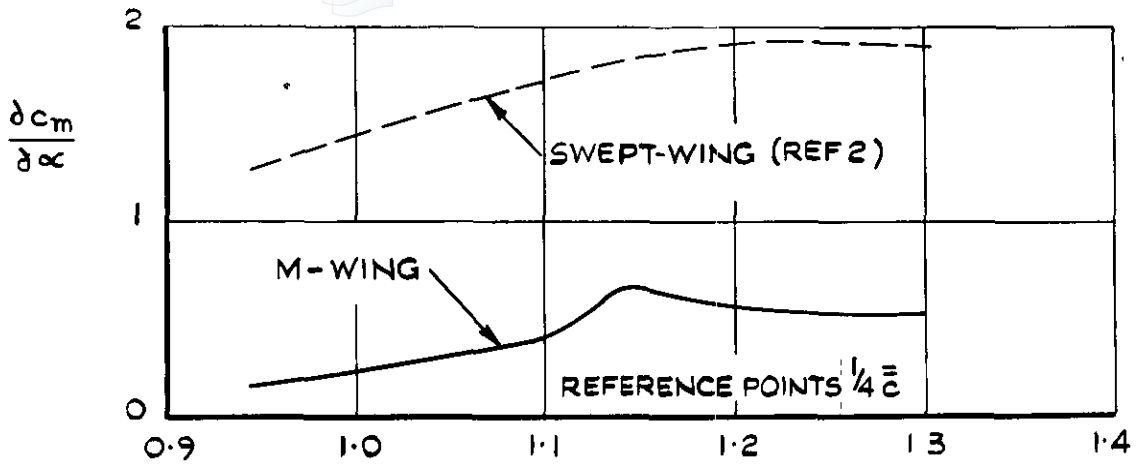
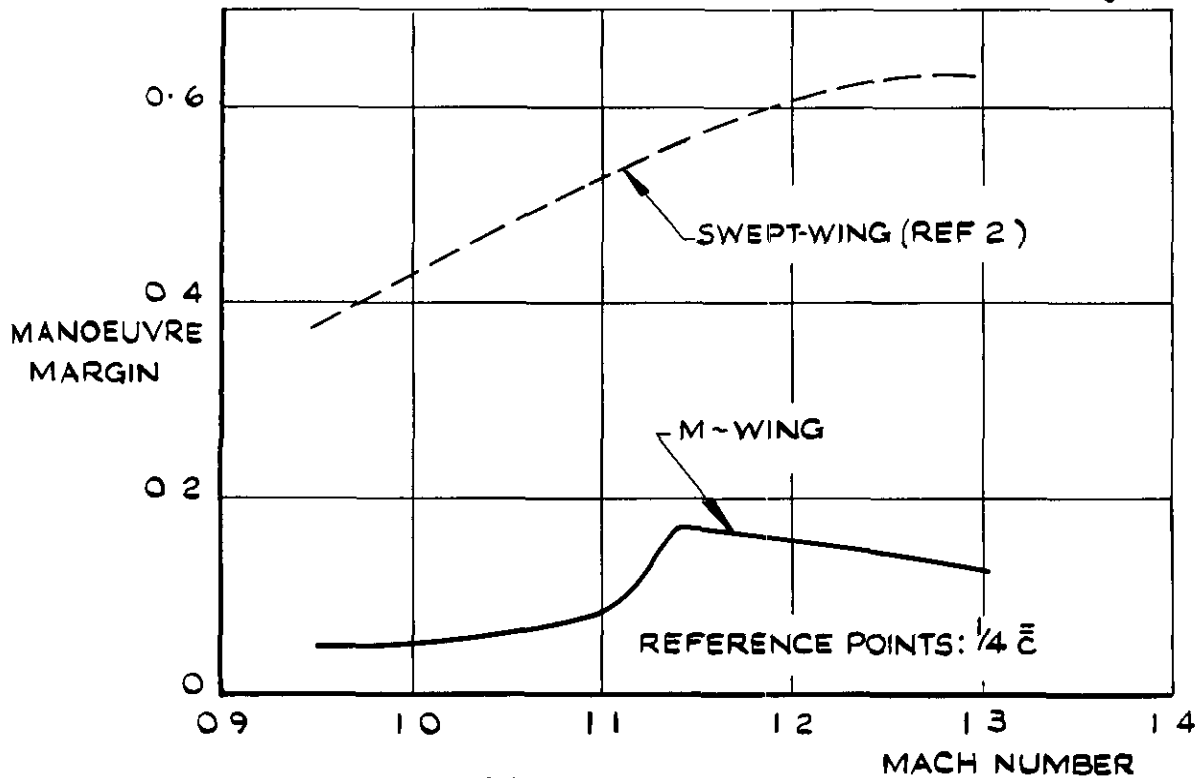


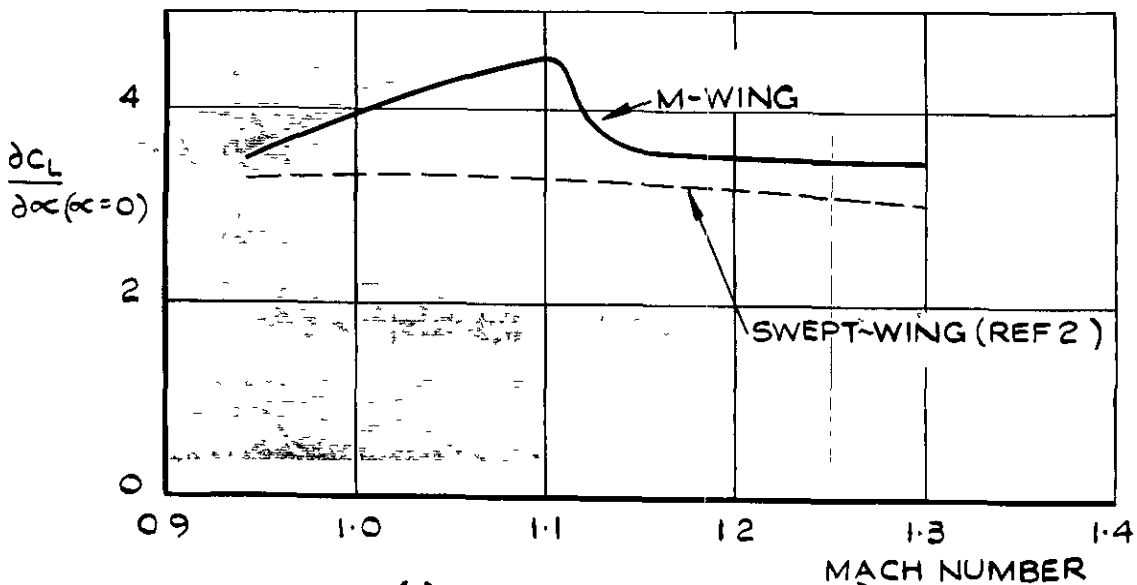
FIG.15. LIFT-CURVE SLOPE AT ZERO INCIDENCE.



(a) PITCHING MOMENT DERIVATIVE  $\frac{\partial c_m}{\partial \alpha} (\alpha=0)$



(b) MANOEUVRE MARGIN



(c) LIFT-CURVE SLOPE  $\frac{\partial c_L}{\partial \alpha} (\alpha=0)$

FIG.16(a.b.c.) COMPARISON BETWEEN STABILITY DERIVATIVES OF M-WING AND SWEPT-WING MODELS.

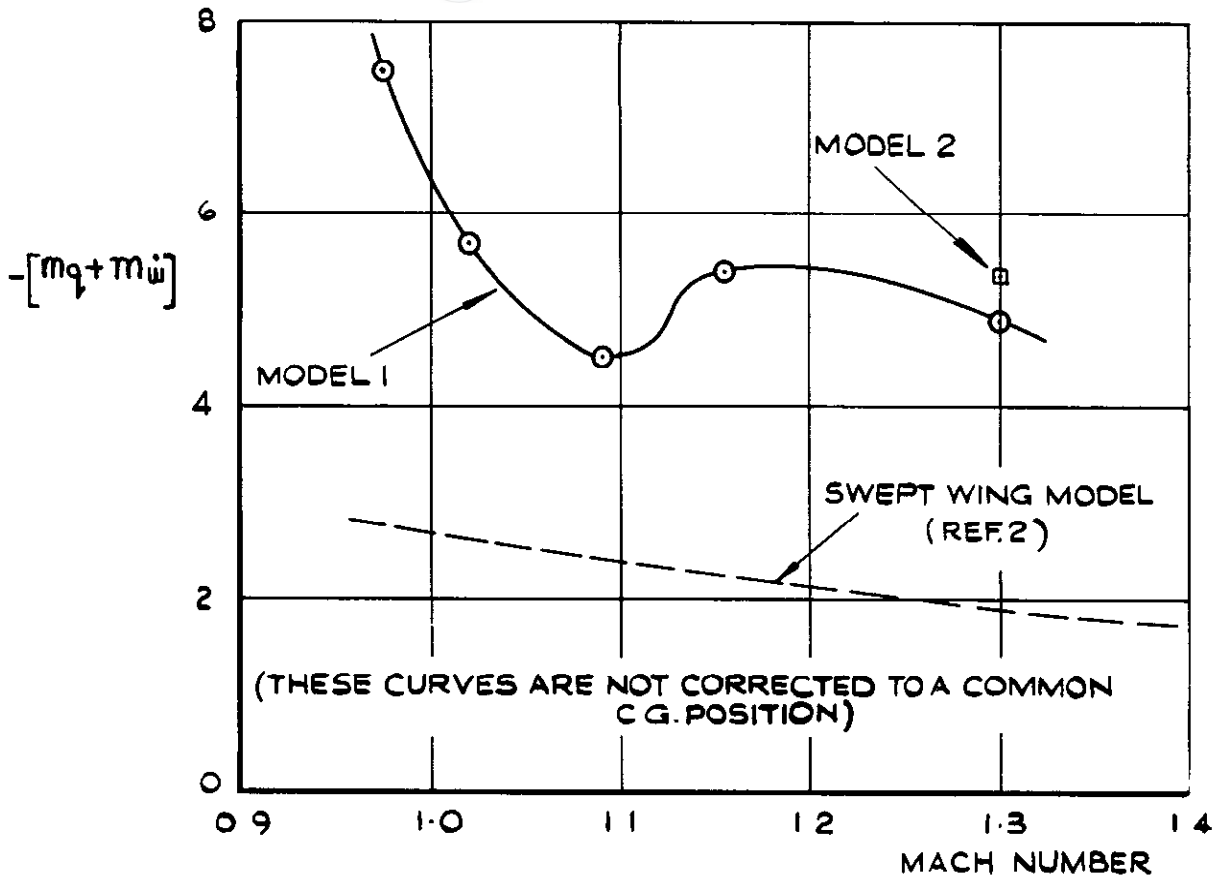


FIG. 17. ROTARY DAMPING IN PITCH  $-[m\ddot{q} + m\dot{\omega}]$

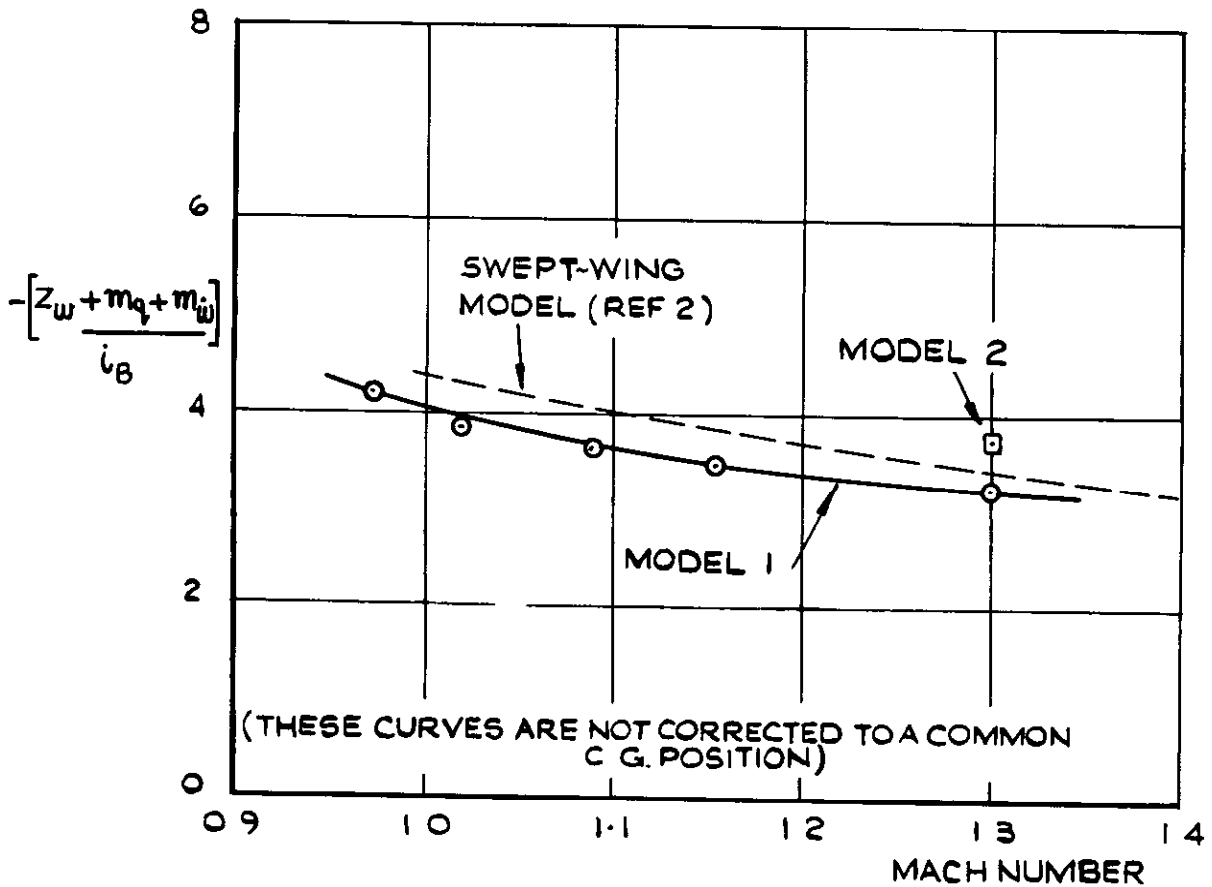


FIG. 18. TOTAL DAMPING IN PITCH  $-\frac{[Z_w + m\ddot{q} + m\dot{\omega}]}{i_B}$

A.R.C. C.P. No. 773

533.693.9:  
533.6.055:  
533.6.013.12:  
533.6.013.412:  
533.6.011.35

FREE-FLIGHT MEASUREMENTS OF THE DRAG AND LONGITUDINAL  
STABILITY OF A TRANSONIC M-WING AIRCRAFT.  
Edwards, J.B.W. November 1963.

Free-flight tests have been made on a model of an M-wing aircraft  
designed to cruise at  $M = 1.2$  with a subsonic type of flow on the wing  
surfaces.

Results are presented for the zero-lift drag and longitudinal  
stability characteristics over the Mach number range from 0.9 to 1.3.

It is shown that the design aims have been achieved in that no  
evidence of shocks in the wing root was found and that some suppression  
of the wing wave drag occurred.

(Over)

A.R.C. C.P. No. 773

533.693.9:  
533.6.055:  
533.6.013.12:  
533.6.013.412:  
533.6.011.35

FREE-FLIGHT MEASUREMENTS OF THE DRAG AND LONGITUDINAL  
STABILITY OF A TRANSONIC M-WING AIRCRAFT.  
Edwards, J.B.W. November 1963.

Free-flight tests have been made on a model of an M-wing aircraft  
designed to cruise at  $M = 1.2$  with a subsonic type of flow on the wing  
surfaces.

Results are presented for the zero-lift drag and longitudinal  
stability characteristics over the Mach number range from 0.9 to 1.3.

It is shown that the design aims have been achieved in that no  
evidence of shocks in the wing root was found and that some suppression  
of the wing wave drag occurred.

(Over)

A.R.C. C.P. No. 773

533.693.9:  
533.6.055:  
533.6.013.12:  
533.6.013.412:  
533.6.011.35

FREE-FLIGHT MEASUREMENTS OF THE DRAG AND LONGITUDINAL  
STABILITY OF A TRANSONIC M-WING AIRCRAFT.  
Edwards, J.B.W. November 1963.

Free-flight tests have been made on a model of an M-wing aircraft  
designed to cruise at  $M = 1.2$  with a subsonic type of flow on the wing  
surfaces.

Results are presented for the zero-lift drag and longitudinal  
stability characteristics over the Mach number range from 0.9 to 1.3.

It is shown that the design aims have been achieved in that no  
evidence of shocks in the wing root was found and that some suppression  
of the wing wave drag occurred.

(Over)

The results are compared with those from free-flight tests on a swept-wing model having the same body, fin and tailplane configuration.

The results are compared with those from free-flight tests on a swept-wing model having the same body, fin and tailplane configuration.

The results are compared with those from free-flight tests on a swept-wing model having the same body, fin and tailplane configuration.



C.P. No. 773

© *Crown Copyright 1964*

Published by  
**HER MAJESTY'S STATIONERY OFFICE**

To be purchased from  
York House, Kingsway, London w c.2  
423 Oxford Street, London w.1  
13A Castle Street, Edinburgh 2  
109 St Mary Street, Cardiff  
39 King Street, Manchester 2  
50 Fairfax Street, Bristol 1  
35 Smallbrook, Ringway, Birmingham 5  
80 Chichester Street, Belfast 1  
or through any bookseller

C.P. No. 773

S.O. CODE No. 23-9015-73